Received: 28 March 2022 | Revised: 1 September 2022 | Accepted: 5 October 2022

DOI: 10.1002/alz.12867

Alzheimer's & Dementia®
THE JOURNAL OF THE ALZHEIMER'S ASSOCIATION

RESEARCH ARTICLE

Functional network segregation is associated with attenuated tau spreading in Alzheimer's disease

Anna Steward[1] | Davina Biel[1] | Matthias Brendel[2,3,4] | Anna Dewenter[1] | Sebastian Roemer[1,5] | Anna Rubinski[1] | Ying Luan[1] | Martin Dichgans[1,3,4] | Michael Ewers[1,3] | Nicolai Franzmeier[1,4] | for the Alzheimer's Disease Neuroimaging Initiative (ADNI)

[1]Institute for Stroke and Dementia Research (ISD), University Hospital, LMU, Munich, Germany

[2]Department of Nuclear Medicine, University Hospital, LMU Munich, Munich, Germany

[3]German Center for Neurodegenerative Diseases (DZNE), Munich, Germany

[4]Munich Cluster for Systems Neurology (SyNergy), Munich, Germany

[5]Department of Neurology, University Hospital, LMU Munich, Munich, Germany

Correspondence
Dr. Nicolai Franzmeier, Institute for Stroke and Dementia Research (ISD), University Hospital, LMU Munich, 81377 Munich, Germany.
E-mail: Nicolai.Franzmeier@med.uni-muenchen.de

Data used in preparation of this article were obtained from the Alzheimer's Disease Neuroimaging Initiative (ADNI) database (adni.loni.usc.edu). As such, the investigators within the ADNI contributed to the design and implementation of ADNI and/or provided data but did not participate in analysis or writing of this report. A complete listing of ADNI investigators can be found at: http://adni.loni.usc.edu/wp-content/uploads/how_to_apply/ADNI_Acknowledgement_List.pdf

Abstract

Introduction: Lower network segregation is associated with accelerated cognitive decline in Alzheimer's disease (AD), yet it is unclear whether less segregated brain networks facilitate connectivity-mediated tau spreading.

Methods: We combined resting state functional magnetic resonance imaging (fMRI) with longitudinal tau positron emission tomography (PET) in 42 betamyloid-negative controls and 81 amyloid beta positive individuals across the AD spectrum. Network segregation was determined using resting-state fMRI–assessed connectivity among 400 cortical regions belonging to seven networks.

Results: AD subjects with higher network segregation exhibited slower brain-wide tau accumulation relative to their baseline entorhinal tau PET burden (typical onset site of tau pathology). Second, by identifying patient-specific tau epicenters with highest baseline tau PET we found that stronger epicenter segregation was associated with a slower rate of tau accumulation in the rest of the brain in relation to baseline epicenter tau burden.

Discussion: Our results indicate that tau spreading is facilitated by a more diffusely organized connectome, suggesting that brain network topology modulates tau spreading in AD.

KEYWORDS
Alzheimer's disease, functional magnetic resonance imaging, network segregation, tau spreading, tau positron emission tomography

Highlights

- Higher brain network segregation is associated with attenuated tau pathology accumulation in Alzheimer's disease (AD).
- A patient-tailored approach allows for the more precise localization of tau epicenters.
- The functional segregation of subject-specific tau epicenters predicts the rate of future tau accumulation.

1 | INTRODUCTION

Alzheimer's disease (AD) is characterized by cerebral amyloid beta (Aβ) plaques and tau tangles. Aβ accumulates decades before symptom manifestation whereas tau pathology develops closely before symptom onset.[1,2] The severity of tau pathology, assessed via tau positron emission tomography (PET) and fluid biomarkers, has been shown to predict subsequent cognitive decline[3–5] suggesting that tau is a key driver of clinical disease progression; hence, it is clinically important to understand the mechanisms that drive the development of tau pathology.

Tau pathology spreads in a characteristic pattern from the medial temporal lobe toward the neocortex,[6] closely followed by neurodegeneration.[7] Preclinical studies have shown that tau spreads via synapses in an activity-dependent manner via anatomical connections rather than seeping into proximal brain regions.[8–10] These findings have recently been translated to biomarker data from AD patients by combining resting state functional magnetic resonance imaging (rs-fMRI) for assessing functional brain connectivity and tau PET imaging for mapping tau pathology spread. Specifically, we and others found that (1) tau pathology distributes preferentially across functionally connected brain regions,[11–13] (2) connected brain regions show correlated tau accumulation rates, and (3) tau pathology emerges in circumscribed epicenters, from where it spreads across functionally connected brain regions.[14–16] Together, these findings provide evidence that the brain's connectome plays an important role in routing tau spread in AD, thereby determining disease progression.

Numerous rs-fMRI studies have revealed that the functional connectome is modular and comprised of functionally specialized networks integral to cognitive functioning.[17,18] Previous studies found that modularity of brain networks diffuses with age resulting in desegregated networks with stronger inter-network connections[19–22] and a general deterioration of functional ability.[23,24] We have shown recently that reduced rs-fMRI–assessed network segregation is linked to stronger cognitive deficits relative to the level of AD pathology in sporadic and inherited AD.[25] Furthermore, modulating effects of network segregation on cognition are supported by longitudinal work, suggesting decreased segregation to be a risk factor for increased severity of dementia symptoms.[26] These studies propose that brain network segregation modulates AD symptom severity by offering resilience toward primary AD pathology, whereby individuals with higher network segregation maintain better cognition despite higher disease burden. However, it is unclear whether higher network segregation only provides resilience against the impact of AD pathology on cognition, or whether higher segregation also attenuates the progression of primary AD pathology, therefore providing resistance against AD pathology. Because tau pathology spreads across connected brain regions,[14–16] it is possible that stronger network segregation restricts inter-regional tau spreading thereby attenuating cognitive decline. Thus, our major aim was to investigate whether stronger network segregation is associated with reduced tau progression and whether a more diffuse network topology is linked to faster tau expansion.

RESEARCH IN CONTEXT

1. **Systematic Review**: Heterogeneity in Alzheimer's disease (AD) progression is problematic for clinical prognosis; therefore, understanding its modulators is highly important. The brain's functional connectome, identified as a critical route for the spreading of connectivity-mediated tau pathology, could be crucial in understanding AD progression.
2. **Interpretation**: Analysis of tau positron emission tomography and resting state functional magnetic resonance imaging data revealed that higher network segregation and higher segregation of patient-specific tau epicenters (onset site of tau pathology) were associated with a slower rate of pathological tau accumulation in the rest of the brain. Findings suggest that a more diffuse network topology facilitates connectivity-mediated inter-regional tau spreading indicating that inter-individual differences in global and tau epicenter connectivity impact the speed of pathological tau progression in AD.
3. **Future Directions**: Using the patient-tailored approach to understand more about the functional heterogeneity of tau epicenters and their specific impact on tau dynamics.

To investigate this, we assessed rs-fMRI and longitudinal flortaucipir tau PET in 81 biomarker-defined AD and 42 control subjects from the Alzheimer's Disease Neuroimaging Initiative (ADNI) database. Our major aim was to assess whether higher network segregation is associated with attenuated tau spreading from brain regions in which tau emerges first (i.e., tau epicenters) to the rest of the brain. Therefore, adhering to the Braak-like stereotypical pattern of tau spreading, we explored first if higher network segregation attenuated the relationship between baseline entorhinal tau burden (i.e., Braak I, the typical site of tau onset), and the rate of tau accumulation in the rest of the brain. Second, we adopted a patient-tailored approach, in which subject-specific tau epicenters were identified as sites with the highest baseline tau PET standardized uptake value ratio (SUVR). We then assessed whether higher segregation of subject-specific tau epicenters was associated with attenuated tau accumulation in the rest of the brain.

2 | METHODS

2.1 | Participants

We included 123 participants from the ADNI database based on availability of longitudinal ^{18}F-flortaucipir tau PET (>1 visit), 3T rs-fMRI and ^{18}F-florbetapir/florbetaben amyloid PET obtained within 6 months of the initial tau PET scan. All subjects were classified as Aβ positive or

negative (Aβ+/−) based on established global 18F-florbetapir (global SUVR > 1.11) and global ^{18}F-florbetaben amyloid PET thresholds (global SUVR > 1.08)[27] applied to amyloid PET SUVR data provided by the ADNI PET core. ADNI investigators diagnosed subjects as either cognitively normal (CN; Mini-Mental State Examination [MMSE] ≥ 24, Clinical Dementia Rating [CDR] = 0, non-depressed), mildly cognitively impaired (MCI; MMSE ≥ 24, CDR = 0.5, objective memory impairment on education-adjusted Wechsler Memory Scale II, preserved activities of daily living) or demented (MMSE = 20–26, CDR > 0.5, National Institute of Neurological and Communicative Disorders and Stroke/Alzheimer's Disease and Related Disorders Association criteria for probable AD). The sample included 42 Aβ− CN subjects and 81 Aβ+ covering the AD spectrum: (CN/MCI/dementia n = 38/25/18); Aβ− subjects with a diagnosis other than CN were excluded owing to suspected non-AD pathology. Ethical approval was obtained by ADNI sites and written informed consent was collected from all participants.

2.2 | MRI and PET acquisition

Structural and functional MRI were acquired using 3T Siemens (SIEMENS Healthineers) and 3T GE scanners. T1-weighted structural scans were collected using a magnetization-prepared rapid gradient echo sequence (repetition time [TR] = 2300 ms; voxel size = 1 × 1 × 1 mm; for parameter details see: https://adni.loni.usc.edu/wp-content/uploads/2017/07/ADNI3-MRI-protocols.pdf). rs-fMRI was obtained using a 3D echo-planar imaging (EPI) sequence with 200 fMRI volumes per subject (TR/echo time [TE] = 3000/30 ms; flip angle = 90°; voxel size = 3.4 × 3.4 × 3.4 mm).

PET data were assessed post–intravenous injection of ^{18}F-labeled tracers (flortaucipir: 6 × 5 minute time frames, 75–105 minutes post-injection; florbetapir: 4 × 5 minute time frames, 50–70 minutes post-injection; florbetaben: 4 × 5 minute time frames, 90–110 minutes post-injection; for more information see http://adni.loni.usc.edu/methods/pet-analysis-method/pet-analysis/).

2.3 | MRI and PET preprocessing

All images were screened for artifacts before preprocessing. T1 scans were skull stripped, bias corrected, segmented, and non-linearly normalized to Montreal Neurological Institute (MNI) space using the advanced normalization tools (ANTs) software package. EPI images were slice-time and motion corrected and co-registered to the native T1-weighted images. Using rigid-transformation parameters, T1-derived gray matter, white matter, and cerebrospinal fluid (CSF) segments were transformed to EPI space. To denoise EPI images, we regressed out nuisance covariates (i.e., white matter and CSF time series plus six motion parameters and their derivatives) and applied detrending and band-pass filtering (0.01–0.08 Hz) in EPI native space. To further reduce movement artifacts that may compromise connectivity assessment[28] we performed motion scrubbing, in which volumes exceeding a 0.5 mm frame-wise displacement threshold were removed, as well as one prior and two subsequent volumes. Subjects for which >30% of volumes had to be removed were not included in the study.[29] Spatial smoothing was not performed to avoid artificially enhancing functional connectivity caused by signal spilling between adjacent brain regions. Preprocessed rs-fMRI images were subsequently normalized to MNI space via T1-derived spatial normalization parameters. To assess the effect of different rs-fMRI processing protocols on our findings, we repeated all analyses further including global signal regression and applying a more restrictive frame-wise displacement threshold of 0.3 mm.

Dynamically acquired tau PET images were realigned and averaged to obtain single flortaucipir images. Using brain-extracted T1-weighted images and ANTs-derived non-linear spatial normalization parameters,[30] tau PET images were affine registered to T1-weighted images, spatially normalized to MNI space, and subsequently intensity normalized using an inferior cerebellar gray reference.[31] Spatially normalized tau PET images were parceled into 400 cortical regions of interest (ROIs) of the Schaefer atlas by averaging ROI-specific voxels (Figure 1A).[32] The atlas was additionally masked using a group-specific gray matter mask binarized at 0.3 probability.

2.4 | Functional connectivity assessment

Functional connectivity was assessed among the 400 ROIs[32] which are grouped into seven major functional networks (Figure 1A), including the default mode network (DMN); ventral attention network (VAN); dorsal attention network (DAN); frontoparietal control network (FPCN); as well as visual, limbic, and motor networks.[33] This atlas was chosen for its suitability for the combination of tau PET and fMRI, owing to the atlas' exclusion of areas outside of the neocortex, which are susceptible to off-target binding of the flortaucipir tracer.[34,35] Fisher z–transformed Pearson-moment correlations of preprocessed ROI-specific rs-fMRI time series were assessed between all possible ROI pairs, and negative values and autocorrelations were set to 0, following our pre-established approach.[25]

2.5 | Network segregation

For the first major analysis, network segregation was calculated according to each ROIs connectivity and its respective network affiliation[33] using a pre-established system segregation (SyS) equation (Equation 1)[19]:

$$SyS = \frac{\overline{zw} - \overline{zb}}{\overline{zw}} \quad (1)$$

whereby zw is the mean within network connectivity and zb is the mean between network connectivity.[19] To ensure that our measure of SyS was not associated with in-scanner motion, we tested the association between SyS and mean framewise displacement during the rs-fMRI scan. Here, no association was found (P = 0.735) using linear regression.

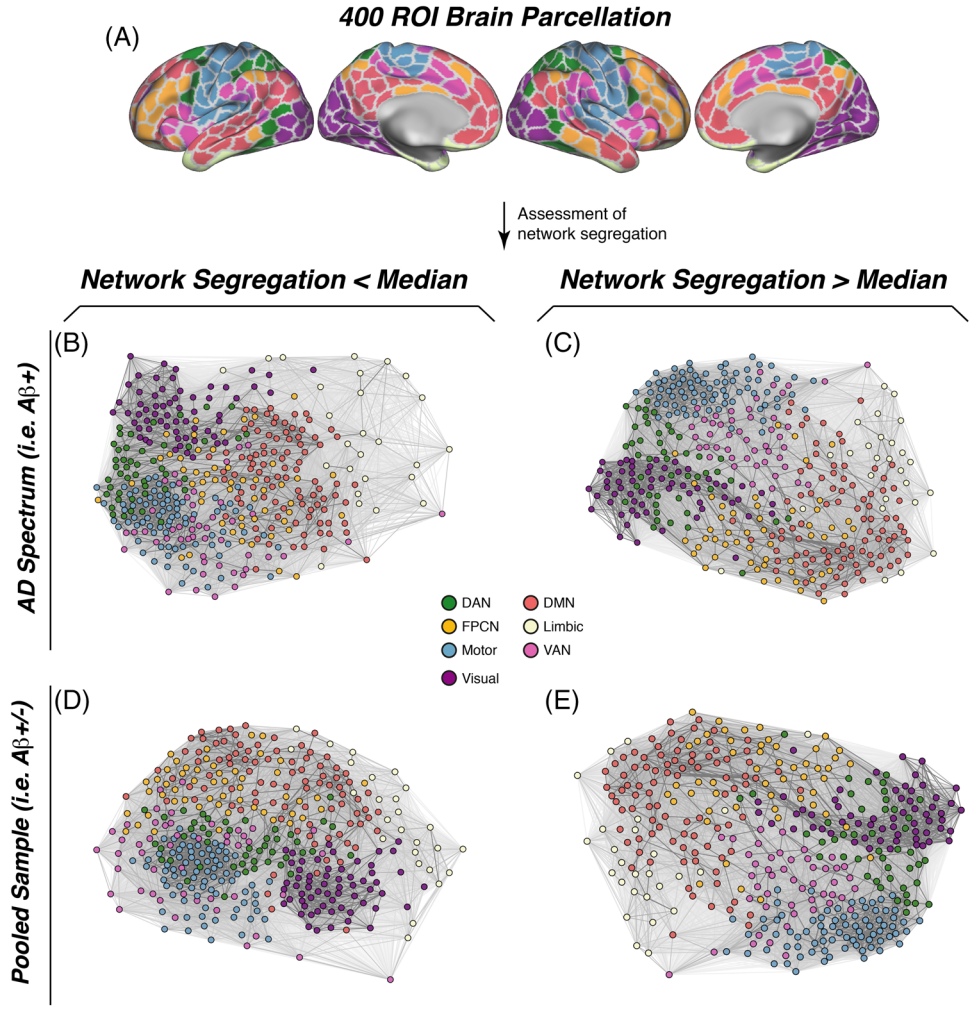

FIGURE 1 The Schaefer 400 region of interest (ROI) brain parcellation grouped into seven major networks was used to determine functional connectivity and network segregation between brain networks (A). Force-directed plots illustrating brain network topology, stratified by amyloid beta positivity (Aβ+: B,C; pooled: D,E) and network segregation level (median split), whereby shorter node distance is representative of higher connectivity strength. Plots were generated using the Fruchtermann–Reingold algorithm applied to group-average functional connectivity data. DAN, dorsal attention network; DMN, default mode network; FPN, frontoparietal control network; VAN, ventral attention network

2.6 | Definition of tau epicenters and epicenter segregation

To assess whether higher segregation of those epicenter regions in which tau is assumed to develop first attenuates the subsequent spreading of tau to the rest of the brain, we determined both the location of tau epicenters as well as the segregation of epicenters for each patient. Epicenters, that is, the potential sites of tau onset in a given individual, were determined for each Aβ+ subject by systematically applying pre-defined tau PET SUVR thresholds to the Schaefer atlas (baseline tau PET SUVRs of 1.3, 1.2, and 1.1).[12,14,16] Subsequently, ROI-wise segregation was defined for each subject, whereby *zw* is the connectivity of a given ROI to all ROIs in its own network and *zb* is the given ROI's connectivity to all other network ROIs as shown in Equation (1). Epicenter segregation was subsequently estimated by averaging the segregation scores of all ROIs belonging to a subject-specific epicenter. Further, we obtained an alternative global measure of network segregation by averaging segregation measures across all 400 ROIs to compare the ROI-wise segregation approach to the whole-brain method used to determine global segregation.[19] Both SyS scores were highly correlated ($r = 0.95$, $R2 = 0.90$, $P < 0.001$) indicating high consistency between the two methods.

2.7 | Statistical analysis

Differences in demographic, cognitive, and PET measures between diagnostic groups were tested using analyses of variance (ANOVAs) for continuous variables and chi-squared (χ^2) tests for categorical variables (Table 1). Annual tau PET change rates were calculated for each ROI by fitting linear mixed models with tau PET SUVR as the dependent variable and time from baseline in years as the independent variable, including random slope and intercept.[36]

To test the main hypothesis of whether higher network segregation attenuates tau spreading, we investigated the interaction effect

TABLE 1 Demographics and sample characteristics

	CN Aβ− (*n* = 42)	CN Aβ+ (*n* = 38)	MCI Aβ+ (*n* = 25)	Dementia Aβ+ (*n* = 18)	*P*-value
Sex (F/M)	26/16	22/16	11/14	6/12	0.151
Age	71.7 (7.24)	74.1 (5.72)	73.4 (6.60)	76.0 (8.26)	0.149
Years of education	16.5 (2.50)	16.5 (2.36)	16.5 (2.76)	15.5 (2.50)	0.511
ADAS13	7.67 (5.01)[c,d]	9.70 (5.43)[d]	15.4 (5.06)[a,d]	26.8 (10.8)[a,b,c]	<0.001
Global tau PET SUVR	1.07 (0.090)[c,d]	1.12 (0.092)[d]	1.22 (0.246)[a,d]	1.40 (0.375)[a,b,c]	<0.001
Annual change in global tau PET SUVR	0.00271 (0.00755)[c,d]	0.00927 (0.0103)[c,d]	0.0183 (0.0163)[a,b]	0.0196 (0.0219)[a,b]	<0.001
Tau PET follow-up in years	1.84 (0.955)	1.84 (0.723)	1.45 (0.499)	1.52 (0.521)	0.098
Centiloid	−4.57 (12.7)[b,c,d]	71.5 (32.9)[a]	82.2 (30.1)[a]	92.0 (37.0)[a]	<0.001
Amyloid PET tracer (florbetapir/florbetaben)	34/8	24/14	15/10	10/8	0.133
SyS	0.507 (0.100)	0.523 (0.083)	0.540 (0.064)	0.514 (0.072)	0.458
rs-fMRI—mean framewise displacement	0.11 (0.06)	0.12 (0.06)	0.08 (0.05)[d]	0.14 (0.06)[c]	0.023

Note: *P*-values were derived from ANOVA for continuous measures and from chi-squared tests for categorical measures. Mean values significantly ($P < 0.05$, Tukey post hoc tests) different from—
[a]CN Aβ−.
[b]CN Aβ+.
[c]MCI Aβ+.
[d]Dementia Aβ+.

between baseline entorhinal tau (i.e., Braak I, the stereotypical site of tau onset of the Braak staging scheme) and global segregation on the rate of longitudinal tau accumulation outside of the entorhinal cortex. To this end, linear models were fit with each subject's baseline entorhinal tau PET SUVR and their global segregation value as well as their interaction as independent variables, and the rate of longitudinal tau change outside of the entorhinal cortex as the dependent variable controlling for age, sex, diagnosis, scanner manufacturer, and mean framewise displacement during the rs-fMRI scan. All interaction effects were computed using continuous measures of tau PET in Braak I and SyS. To understand the influence of network segregation on distinct stages of tau expansion, further exploratory linear models using the same covariates as described above were fitted to isolate the effect of higher network segregation and entorhinal tau (i.e., Braak I) on tau change rates in earlier affected areas, Braak stages III and IV, and in the last affected areas, Braak stages V and VI. To assess the robustness of the interaction effects and to ensure that our results were not biased by influential cases, we recomputed all above-described models using 1000 bootstrapped samples (i.e., a random sample with replacement is drawn from the overall sample for each bootstrapping iteration) and determined 95% confidence intervals of the interaction effect beta values.

Our second aim was to explore whether higher segregation of patient-specific tau epicenters, not necessarily confined to the entorhinal cortex, limited the rate of tau accumulation outside of the epicenter, using baseline tau PET SUVRs of individualized tau epicenters at different thresholds and average annual tau PET accumulation across ROIs outside of the epicenter. To define epicenters, we selected brain regions that surpassed a pathological threshold of a tau PET SUVR > 1.3 at baseline, to ensure that epicenters are confined to regions with actual tau pathology. We further repeated this analysis using more liberal epicenter thresholds (i.e., SUVRs > 1.2 or 1.1), to assess whether the interaction effect becomes weaker if also regions with less tau pathology are included, which should be less influential for tau accumulation in the rest of the brain. A linear model was fitted taking each subject's epicenter tau PET SUVR value, epicenter segregation value, and their interaction as the independent variables and the rate of longitudinal tau change outside of the epicenter as the dependent variable controlling for age, sex, diagnosis, scanner manufacturer, and mean framewise displacement during the rs-fMRI scan. To further explore the effect of epicenter size on the interaction between epicenter segregation and tau PET SUVR on the rate of tau spreading, linear models with the same variables were repeated at different epicenter thresholds systematically varied between tau PET SUVRs of 1.0 to 1.3 in steps of 0.01. The standardized beta value of the interaction effect (epicenter segregation x epicenter tau PET SUVR) was extracted from each linear model and correlated with epicenter SUVR threshold to assess whether interaction effects weakened at more liberal epicenter definitions. All statistical analyses were conducted in R. All analyses were repeated across different rs-fMRI preprocessing protocols, including or excluding global signal regression and applying different framewise displacement thresholds of 0.5 mm and 0.3 mm.

2.8 | Data availability

ADNI data are publicly available (adni.loni.usc.edu) upon registration and compliance with the data use agreement. The data that support the findings of this study are available on reasonable request from the

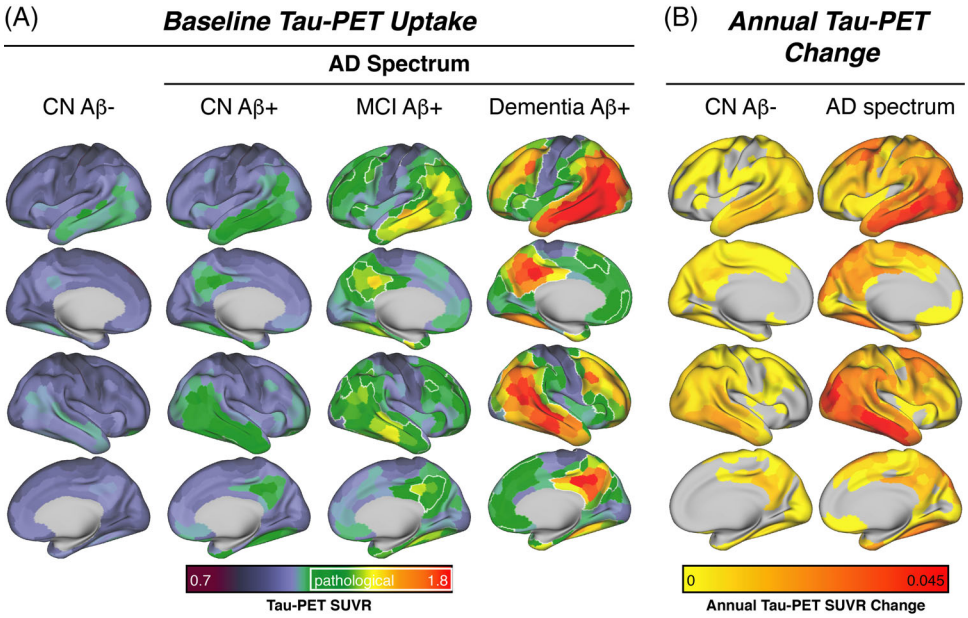

FIGURE 2 Group-average tau PET SUVRs at baseline stratified by amyloid status and diagnostic group. Tau PET SUVRs are shown as continuous values, white outlines define areas which surpass a pre-established pathological tau SUVR threshold of 1.3[58] (A). Group average tau SUVR annual change rates defined by linear mixed models, stratified by amyloid positivity (B). AD, Alzheimer's disease; CN, cognitively normal; MCI, mild cognitive impairment; PET, positron emission tomography; SUVR, standardized uptake volume ratio

corresponding author. The analysis R code can be found in the supporting information.

3 | RESULTS

3.1 | Sample characteristics

A total of 123 subjects were included in the study, of which 81 were classified as Aβ+ and diagnosed within the AD spectrum, versus 42 Aβ− CN controls. ANOVAs and χ^2 tests revealed no significant differences in baseline demographics (i.e., age, sex, education) or tau- PET follow-up times, but the expected group differences in baseline tau PET SUVRs ($F[3,119] = 13.64$, $P < 0.001$), annual tau PET change rates ($F[3,119] = 10.78$, $P < 0.001$), amyloid PET levels ($F[3,119] = 86.69$, $P < 0.001$), and global cognition (i.e., Alzheimer's Disease Assessment Scale 13-item cognitive subscale, $F[3,119] = 11.71$, $P < 0.001$). All group characteristics and the directionality of group differences are summarized in Table 1. When mapping the spatial pattern of tau PET uptake and annual tau PET change rates across groups, increasing AD severity was associated with stronger temporoparietal and frontal tau deposition (Figure 2A) and AD groups showed faster temporoparietal tau accumulation than controls (Figure 2B). No significant difference was found for global network segregation (i.e., SyS) across groups ($F[3,119] = 0.871$, $P = 0.458$). Force-directed plots for illustrating brain network topologies in the pooled and AD spectrum sample are shown in Figure 1B,E.

3.2 | Higher network segregation attenuates the association between entorhinal tau PET and tau accumulation in the rest of the brain

To test our main hypothesis of whether a more segregated brain network topology is associated with attenuated tau spreading from Braak I (i.e., entorhinal cortex) to Braak III to VI regions (Figure 3A), we tested whether higher global network segregation (i.e., SyS) attenuated the rate of tau spreading from the entorhinal cortex to the rest of the brain in Aβ+. Supporting this, results revealed an interaction between SyS and baseline entorhinal tau PET SUVRs on the subsequent tau accumulation rate in Braak III through VI regions in Aβ+ ($\beta = -2.11$, $P = 0.023$; Figure 3B). Specifically, at a given level of entorhinal tau PET, subjects with higher network segregation had slower rates of tau accumulation in Braak III through VI regions. Congruent effects were found when exploratorily investigating this association in separate Braak-stage ROIs. Specifically, we found significant interaction effects between SyS and entorhinal tau PET SUVRs on the rate of tau accumulation in Braak III and IV ($\beta = -2.17$ $P = 0.027$; Figure 3C) and Braak V and VI ROIs ($\beta = -2.01$, $P = 0.024$; Figure 3D). All findings were consistent but less pronounced when the same analysis was repeated in the pooled Aβ− and Aβ+ sample in Braak III through VI ($\beta = -1.44$, $P = 0.033$; Figure 3E), Braak III and IV ($\beta = -1.33$, $p = .056$; Figure 3F) and Braak V and VI ROIs ($\beta = -1.44$, $P = 0.028$; Figure 3G). All results were non-parametrically confirmed by bootstrapping. Detailed statistics including bootstrapped confidence intervals and R^2 values are summarized in Table 2. Further, all results remained consistent when repeated across

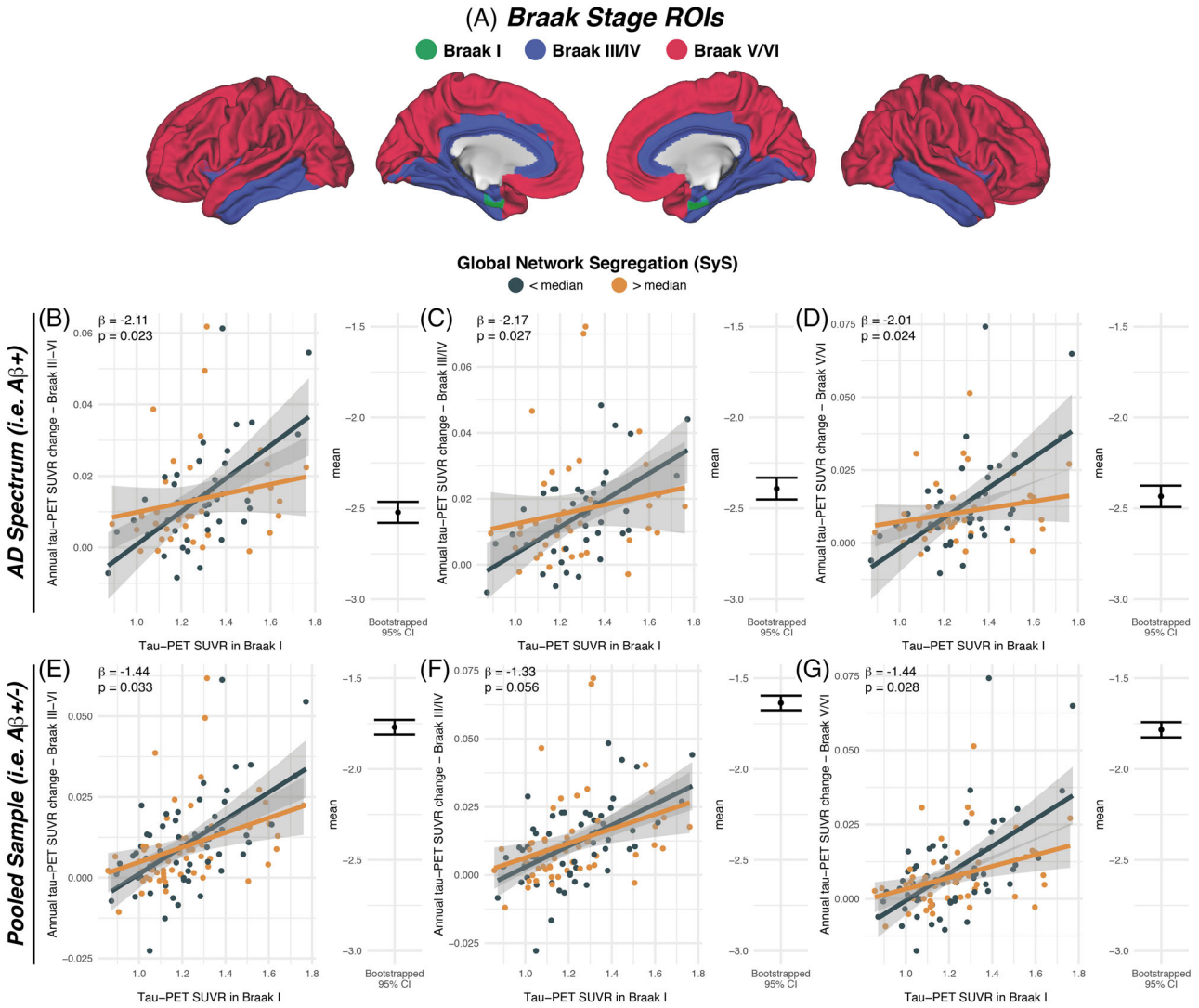

FIGURE 3 Surface rendering of the Braak-staging regions of interest (ROIs) that were applied to tau positron emission tomography (PET) data to determine baseline tau PET levels and longitudinal tau PET changes (A). Scatterplots illustrating the interaction effect between global network segregation (SyS) and entorhinal tau PET levels at baseline on tau PET increase in the remaining brain for amyloid beta positivity (Aβ+), showing that higher network segregation is associated with an attenuated association between entorhinal tau PET and tau accumulation in the rest of the brain (B). Exploratory analyses were performed in Aβ+ subjects, testing the same regression models for earlier Braak regions III/IV (C) and late Braak regions V/VI (D). Analyses were repeated also including the Aβ− control group (E–G). All statistical tests were fitted with continuous data, the use of median split to divide subjects is solely for visual purposes. 95% confidence intervals of interaction effects determined on 1000 bootstrapped iterations are displayed next to each scatterplot. SUVR, standardized uptake value ratio

different rs-fMRI preprocessing protocols (Table S1 in supporting information).

3.3 | Epicenter segregation attenuates tau spreading in AD

Next, we investigated whether the segregation of patient-specific tau epicenters affects subsequent tau accumulation in the rest of the brain in AD. This aim was motivated by evidence for heterogeneous tau spatial distribution patterns that deviate from the stereotypical Braak staging pattern.[14,37,38] To illustrate heterogeneity in tau epicenters, we rendered tau epicenter probabilities across different epicenter thresholds (i.e., tau PET SUVRs > 1.3/1.2/1.1; Figure 4A,C,E) in Aβ+. Linear models for epicenters across varying epicenter thresholds revealed that the interaction of epicenter segregation and the level of baseline epicenter tau SUVR significantly predicted the rate of tau accumulation outside of the epicenter. Specifically, Aβ+ subjects with higher epicenter segregation had slower annual tau accumulation rates in non-epicenter regions at an epicenter tau PET SUVR threshold > 1.3 ($\beta = -4.283$, $P = 0.003$, Figure 4B); however, the effects became statistically weaker at more liberal epicenter thresholds (tau PET SUVR > 1.2: $\beta = -2.754$, $P = 0.014$, Figure 4D; tau PET SUVR > 1.1: $\beta = -2.460$, $P = 0.024$, Figure 4F). Detailed statistics including bootstrapped

TABLE 2 Interaction effects of baseline tau PET in Braak I times SyS on tau PET rate of change in downstream Braak ROIs (i.e., Braak III-VI)

Group	Tau PET ROC in	*β*-value	*t*-value	*P*-value	Partial *R*2	Bootstrapped beta (mean [95% CI])
A*β*+	Braak III–VI	−2.11	−2.330	0.023	0.070	−2.434 [−2.493; −2.375]
	Braak III–IV	−2.17	−2.267	0.027	0.067	−2.391 [−2.451; −2.331]
	Braak V–VI	−2.01	−2.311	0.024	0.069	−2.433 [−2.493; −2.375]
A*β*+/A*β*− pooled	Braak III–VI	−1.44	−2.164	0.033	0.039	−1.769 [−1.809; −1.729]
	Braak III–IV	−1.33	−1.927	0.056	0.032	−1.636 [−1.677; −1.596]
	Braak V–VI	−1.44	−2.225	0.028	0.042	−1.783 [−1.825; −1.742]

Note: All statistics are based on linear models that were controlled for age, sex, diagnosis, scanner manufacturer, and mean framewise displacement during the resting-state fMRI scan. Regression weights are displayed as standardized beta values. Interaction effects have been computed using continuous measures of SyS and tau PET SUVRs in Braak I. Bootstrapping of interaction effects was performed using 1000 iterations to determine 95% confidence intervals. Confidence intervals not including zero provide non-parametric evidence for the significance of effects.

Abbreviations: A*β*, amyloid beta; CI, confidence interval; PET, positive emission tomography; fMRI, functional magnetic resonance imaging; ROC, receiver operating characteristic; ROIs, regions of interest; SUVR, standardized uptake value ratio; SyS, system segregation.

confidence intervals and R^2 values are summarized in Table 3. Further, all analyses remained consistent across different fMRI preprocessing protocols (Table S2 in supporting information). In addition, we performed null-model analyses, to test the specificity of epicenter tau PET and segregation as a predictor of tau PET change in remaining brain regions. To this end, we assessed the interaction between baseline tau PET in the non-epicenter and segregation of the non-epicenter on subsequent tau PET change rates in the tau epicenter. As expected, we did not find significant interaction effects across different thresholds (tau PET SUVR 1.3/1.2/1.1, $P = 0.23/0.47/0.63$), supporting the view that specifically epicenter regions with high tau pathology at baseline are informative for tau accumulation in remaining brain regions with low tau, and that higher segregation of the epicenter attenuates this association. To systematically investigate whether the effect of epicenter thresholds on the interaction effect between epicenter tau PET and epicenter segregation on tau accumulation in the rest of the brain weakened if epicenters were defined more liberally, we repeated this analysis while systematically reducing epicenter thresholds from tau PET SUVRs of 1.3 to 1.0 in steps of 0.01. In line with the previous analyses, interaction effects became weaker at more liberal epicenter definitions; that is, moving from higher to lower epicenter tau PET thresholds (Figure 5). This result pattern was mirrored in a negative association between epicenter thresholds and the strength of the interaction effect (i.e., beta value) between epicenter segregation and epicenter tau PET on the tau PET rate of change outside of the epicenter ($\beta = -0.81$, $P < 0.001$). Again, this result was consistent across different fMRI preprocessing protocols (Table S3 in supporting information).

4 | DISCUSSION

Our major finding was that higher segregation of functional brain networks is associated with attenuated tau accumulation in AD. Using rs-fMRI, we determined network segregation among seven major brain networks and found that individuals with higher network segregation exhibited a weaker association between baseline tau PET in the entorhinal cortex and the rate of tau accumulation in the rest of the brain. This finding, in line with the concept of connectivity-mediated tau spreading, conveys that inter-regional tau spreading is restricted by the sparser inter-network connections associated with stronger network segregation. Second, by identifying individualized tau epicenters as sites of patient-specific tau onset, we demonstrated that epicenter segregation similarly impacts heterogeneous tau spreading patterns, whereby individuals with higher epicenter segregation exhibited attenuated tau accumulation in the rest of the brain.

Our major finding that higher global network segregation is associated with an attenuated rate of pathological tau spreading in AD further reinforces preclinical evidence and extends translational research by supporting activity-dependent trans-neuronal tau spreading. Translational research revealed that the more connected a brain region is, the more vulnerable it is to tau pathology[11,12,38] and regions functionally connected to areas harboring tau are more likely to also harbor tau, regardless of spatial proximity.[14] We substantiate the concept of functional connectivity-related tau vulnerability introduced by these previous studies by demonstrating that the abundance and dispersion of functional connections are related to the ease of tau spreading.

Second, we demonstrate that tau accumulation can be determined by the segregation of subject-specific tau epicenters. In accordance with our first finding, we show that higher epicenter segregation is similarly related to curbed tau vulnerability, whereby high epicenter segregation may act as a barrier keeping tau more restricted to the epicenter. Additionally, we identify that defining an epicenter as a region with an abnormally high baseline tau load (i.e., SUVR > 1.3) holds the most predictive power about an individual's impending AD progression by illustrating a deterioration of the epicenter's predictive power as it is defined more liberally. These findings illustrate how regions that harbor less tau at baseline explain little about future tau progression, thereby emphasizing the importance of defining epicenters precisely as regions harboring significant tau pathology to maximize the model's strength for predicting patient-level future tau accumulation. Further, it is clear from previous studies that regional variability in tau deposition exists in AD;[14,37] therefore, assuming stereotypical tau deposition

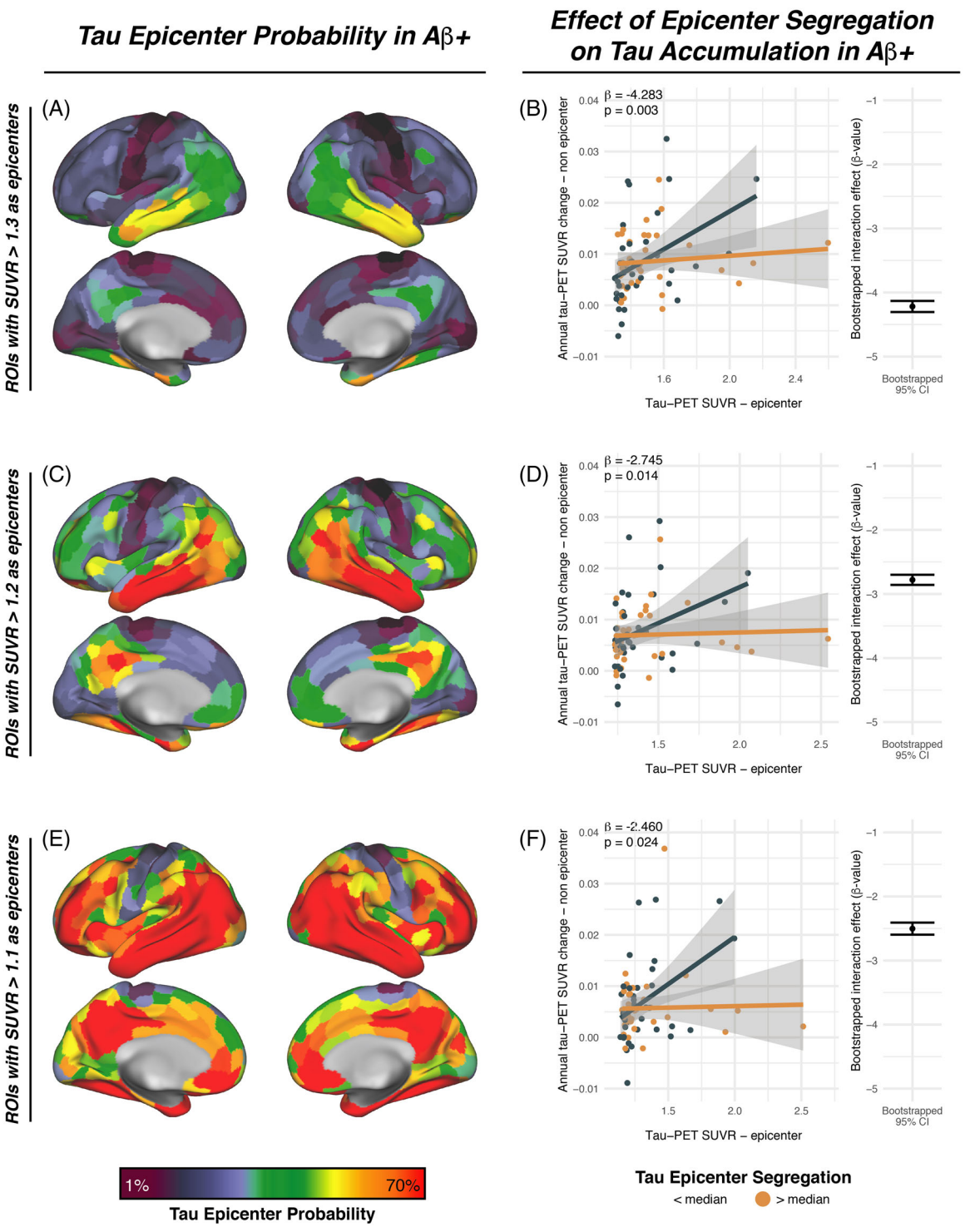

FIGURE 4 Illustration of the association between baseline tau positron emission tomography (PET) in patient-specific tau epicenters and resting state functional magnetic resonance imaging–assessed epicenter segregation on the longitudinal tau PET increase in the remaining non-epicenter regions of interest (ROIs) in amyloid beta positive (Aβ+) subjects. When retaining ROIs above 1.3 tau PET standardized uptake value ratios (SUVRs) as tau epicenters (i.e., 10 ROIs), the highest epicenter probability is found in the inferior temporal lobe, as illustrated by the epicenter probability mapping (A). Regression analyses revealed that higher segregation of the epicenter was associated with slower longitudinal tau PET increase outside of the tau epicenter (B). Analyses were repeated for epicenter tau PET SUVR thresholds of 1.2 (C,D) and 1.1 (E,F), showing that the effect of epicenter segregation decreases statistically if tau epicenters are defined more liberally. All statistical tests were fitted with continuous data, the use of median split to divide subjects is solely for visual purposes. 95% confidence intervals of interaction effects determined on 1000 bootstrapped iterations are displayed next to each scatterplot

TABLE 3 Interaction effects of baseline tau PET in the tau epicenter on tau PET rate of change in non-epicenter ROIs across different epicenter thresholds in Aβ+ subjects

		B	*t*-value	*P*-value	Partial R^2	Bootstrapped beta (mean [95% CI])
Tau PET ROC in epicenter defined as ROIs above a tau-PET SUVR threshold of	SUVR > 1.3	−4.283	−3.041	0.003	0.126	−4.218 [−4.305; −4.131]
	SUVR > 1.2	−2.745	−2.532	0.014	0.091	−2.779 [−2.858; −2.7]
	SUVR > 1.1	−2.460	−2.313	0.024	0.077	−2.502 [−2.597; −2.408]

Note: All statistics are based on linear models that were controlled for age, sex, diagnosis, scanner manufacturer, and mean framewise displacement during the resting-state fMRI scan. Regression weights are displayed as standardized beta values. Interaction effects have been computed using continuous measures of epicenter segregation and epicenter tau PET SUVRs. Bootstrapping of interaction effects was performed using 1000 iterations to determine 95% confidence intervals. Confidence intervals not including zero provide non-parametric evidence for the significance of effects.

Abbreviations: CI, confidence interval; PET, positive emission tomography; fMRI, functional magnetic resonance imaging; ROIs, regions of interest; SUVR, standardized uptake value ratio.

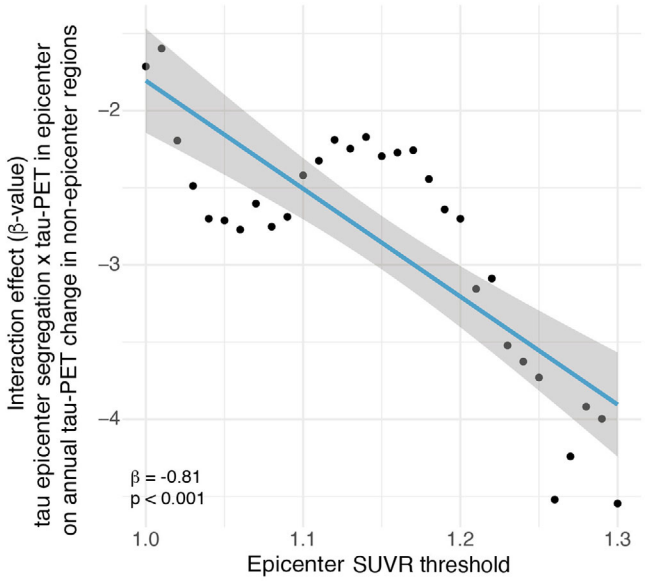

FIGURE 5 Standardized beta values reflecting the interaction between epicenter tau positron emission tomography (PET) standardized uptake value ratios (SUVRs) and resting state functional magnetic resonance imaging–assessed epicenter segregation on the rate of tau accumulation in non-epicenter regions of interest (ROIs) were extracted from linear models fitted with epicenter SUVR thresholds ranging between 1.0 to 1.3 in steps of 0.01. The scatterplot maps out the interaction effect strengths according to epicenter threshold to illustrate the weakening interaction effect as epicenters are defined more liberally, that is, epicenter segregation better predicts tau accumulation when the epicenter is defined more restrictively. All beta values were determined using linear regression

patterns may bias predictions about impending tau progression for individuals with heterogeneous onset sites. Based on our findings, we reason that an individualized approach could be essential in paving the way toward patient-tailored models for predicting tau progression in AD.

Empirical work preceding ours provides support for an association between network segregation and cognitive functioning in AD.[25,26] Specifically, these studies suggest that network segregation provides resilience against the impact of AD primary pathology on cognition whereby individuals are able to maintain higher functional and cognitive ability regardless of pathological burden. Our findings, on the other hand, demonstrate that network segregation also provides resistance against AD pathology by impeding tau spreading.[39] In line with evidence that tau is the key driver of cognitive decline in AD,[3–5] our findings provide a mechanistic intermediary process by which network segregation could modulate prospective tau spreading and thus cognitive outcomes in AD. It is important to mention that our results do not mitigate the protective role of network segregation against cognitive decline in terms of cognitive resilience; indeed, we believe there are inarguable protective effects of network segregation that are determined long before the onset of tau pathology (e.g., Chan et al.[26]) which offer alternative clinical utility for attenuating AD progression and attractive motivation for future research. A key open question for future research will be to assess whether inter-individual differences in brain network segregation persist throughout the lifespan and which factors may have caused such differences. Here, previous studies have related higher education to higher segregation in older adults[40] while stronger vascular brain changes have been linked to lower brain network segregation,[41] which may explain why patients with vascular co-pathology are more prone to tau accumulation in AD.[42] Here, life span studies will be needed to address potential genetic,[43] lifestyle,[40,44] and age-specific factors[45] that influence segregation, which will be important to assess whether brain network segregation can in fact be modulated to potentially attenuate tau accumulation and spreading in AD.

Various caveats should be taken into account when interpreting our results. First, unspecific flortaucipir off-target binding is common place[46] and we have therefore compensated for it by excluding particularly problematic regions such as the hippocampus and basal ganglia. Although the exclusion of known off-target binding sites may reduce confound considerably, off-target binding can still occur elsewhere in the brain and it is therefore impossible to completely eliminate its confound from our analyses. In addition, owing to the exclusion of certain brain regions we cannot confirm that critical stages of tau spreading were not missed; a particular ROI, the hippocampus, an early site of tau pathology,[47,48] unfortunately cannot be explored with first-generation tau PET tracers. Second, functional connectivity reflects direct but also indirect neuronal connections, whereby multiple intermediary neu-

rons are involved.[49,50] The assumptions made in this study rely on the accurate mapping of tau PET to functional connectivity, which unfortunately cannot be fully backed by structural data owing to present-day methodological drawbacks.[51] Therefore, any complex multi-synaptic connections captured by our functional connectivity analysis anticipates confirmation from modern structural techniques that are able to pick up distanced cortico-cortical connections.

Third, our longitudinal AV1451 tau PET analysis was carried out without partial volume correction (PVC) owing to insufficient temporally corresponding MR images. Previous research demonstrates that longitudinal changes in AV1451 tau PET can be accurately measured without PVC;[52,53] therefore, we believe that our longitudinal findings accurately reflect tau accumulation patterns. Finally, although our results follow on from previous preclinical and translational research, we of course recommend validation using another sample from the AD population before generalization, once sufficient data become publicly available.

Together, the current study revealed that higher network segregation is associated with attenuated tau spreading and demonstrates the impact of inter-individual differences in the tau epicenter's and the functional connectome's organization on AD progression. These findings add to the growing literature on factors that may modulate tau spreading, including sex, physical activity, and genetic factors.[42,54–57] Here, it will be important for future studies to systematically assess the individual and potentially synergistic effects of modulators of tau pathology to develop patient-tailored approaches to attenuate the development of tau pathology on the individual level, which may hold promise for attenuating neurodegeneration and cognitive decline in AD. In addition, our findings hold value for clinical research as they promote the brain's complex network topology as a therapeutic target and bring the functional properties of the tau epicenter into focus for future investigations, and not exclusively in AD, but potentially in other tauopathies.

ACKNOWLEDGMENTS

Data collection and sharing for this project was funded by the Alzheimer's Disease Neuroimaging Initiative (ADNI; National Institutes of Health Grant U01 AG024904) and DOD ADNI (Department of Defense award number W81XWH-12-2-0012). ADNI is funded by the National Institute on Aging, the National Institute of Biomedical Imaging and Bioengineering, and through generous contributions from the following: AbbVie; Alzheimer's Association; Alzheimer's Drug Discovery Foundation; Araclon Biotech; BioClinica, Inc.; Biogen; Bristol-Myers Squibb Company; CereSpir, Inc.; Cogstate; Eisai Inc.; Elan Pharmaceuticals, Inc.; Eli Lilly and Company; EuroImmun; F. Hoffmann-La Roche Ltd and its affiliated company Genentech, Inc.; Fujirebio; GE Healthcare; IXICO Ltd.; Janssen Alzheimer Immunotherapy Research & Development, LLC; Johnson & Johnson Pharmaceutical Research & Development LLC; Lumosity; Lundbeck; Merck & Co., Inc.; Meso Scale Diagnostics, LLC; NeuroRx Research; Neurotrack Technologies; Novartis Pharmaceuticals Corporation; Pfizer Inc.; Piramal Imaging; Servier; Takeda Pharmaceutical Company; and Transition Therapeutics. The Canadian Institutes of Health Research is providing funds to support ADNI clinical sites in Canada. Private sector contributions are facilitated by the Foundation for the National Institutes of Health (www.fnih.org). The grantee organization is the Northern California Institute for Research and Education, and the study is coordinated by the Alzheimer's Therapeutic Research Institute at the University of Southern California. ADNI data are disseminated by the Laboratory for Neuro Imaging at the University of Southern California. The study was funded by grants from the LMU (FöFoLe, 1032, awarded to NF, FöFoLe, 1119 awarded to DB), the Hertie foundation for clinical neurosciences (awarded to NF), the SyNergy excellence cluster (EXC 2145/ID 390857198) and the German Research Foundation (DFG, INST 409/193-1 FUGG).

Open access funding enabled and organized by Projekt DEAL.

CONFLICTS OF INTEREST

The authors report no competing interests. Author disclosures are available in the supporting information.

REFERENCES

1. Scholl M, Lockhart SN, Schonhaut DR, et al. PET imaging of tau deposition in the aging human brain. *Neuron*. 2016;89:971-82.
2. Jack CR, Jr., Knopman DS, Jagust WJ, et al. Hypothetical model of dynamic biomarkers of the Alzheimer's pathological cascade. *Lancet Neurol*. 2010;9:119-28.
3. Cullen NC, Leuzy A, Janelidze S, et al. Plasma biomarkers of Alzheimer's disease improve prediction of cognitive decline in cognitively unimpaired elderly populations. *Nat Commun*. 2021;12:3555.
4. Ossenkoppele R, Smith R, Mattsson-Carlgren N, et al. Accuracy of tau positron emission tomography as a prognostic marker in preclinical and prodromal Alzheimer disease: a head-to-head comparison against amyloid positron emission tomography and magnetic resonance imaging. *JAMA Neurol*. 2021;78:961-71.
5. Biel D, Brendel M, Rubinski A, et al. Tau-PET and in vivo Braak-staging as prognostic markers of future cognitive decline in cognitively normal to demented individuals. *Alzheimers Res Ther*. 2021;13:137.
6. Braak H, Braak E. Neuropathological stageing of Alzheimer-related changes. *Acta Neuropathol*. 1991;82:239-59.
7. La Joie R, Visani AV, Baker SL, et al. Prospective longitudinal atrophy in Alzheimer's disease correlates with the intensity and topography of baseline tau-PET. *Sci Transl Med*. 2020;12.
8. Calafate S, Buist A, Miskiewicz K, et al. Synaptic contacts enhance cell-to-cell tau pathology propagation. *Cell Report*. 2015;11:1176-83.
9. De Calignon A, Polydoro M, Suárez-Calvet M, et al. Propagation of tau pathology in a model of early Alzheimer's disease. *Neuron*. 2012;73:685-97.
10. Ahmed Z, Cooper J, Murray TK, et al. A novel in vivo model of tau propagation with rapid and progressive neurofibrillary tangle pathology: the pattern of spread is determined by connectivity, not proximity. *Acta Neuropathologica*. 2014;127:667-83.
11. Cope TE, Rittman T, Borchert RJ, et al. Tau burden and the functional connectome in Alzheimer's disease and progressive supranuclear palsy. *Brain*. 2018;141:550-67.
12. Franzmeier N, Rubinski A, Neitzel J, et al. Functional connectivity associated with tau levels in ageing, Alzheimer's, and small vessel disease. *Brain*. 2019;142:1093-107.
13. Vogel JW, Iturria-Medina Y, Strandberg OT, et al. Spread of pathological tau proteins through communicating neurons in human Alzheimer's disease. *Nat Commun*. 2020;11:2612.
14. Franzmeier N, Dewenter A, Frontzkowski L, et al. Patient-centered connectivity-based prediction of tau pathology spread in Alzheimer's disease. *Sci Adv*. 2020;6.

15. Adams JN, Maass A, Harrison TM, Baker SL, Jagust WJ. Cortical tau deposition follows patterns of entorhinal functional connectivity in aging. *Elife*. 2019;8.
16. Franzmeier N, Neitzel J, Rubinski A, et al. Functional brain architecture is associated with the rate of tau accumulation in Alzheimer's disease. *Nat Commun*. 2020;11:347.
17. Sporns O, Betzel RF. Modular brain networks. *Annu Rev Psychol*. 2016;67:613-40.
18. Wig GS. Segregated systems of human brain networks. *Trends Cogn Sci*. 2017;21:981-96.
19. Chan MY, Park DC, Savalia NK, Petersen SE, Wig GS. Decreased segregation of brain systems across the healthy adult lifespan. *Proc Natl Acad Sci U S A*. 2014;111:E4997-5006.
20. Betzel RF, Byrge L, He Y, Goñi J, Zuo X-N, Sporns O. Changes in structural and functional connectivity among resting-state networks across the human lifespan. *Neuroimage*. 2014;102:345-57.
21. Chong JSX, Ng KK, Tandi J, et al. Longitudinal changes in the cerebral cortex functional organization of healthy elderly. *J Neurosci*. 2019;39:5534-50.
22. Meunier D, Achard S, Morcom A, Bullmore E. Age-related changes in modular organization of human brain functional networks. *Neuroimage*. 2009;44:715-23.
23. Chan MY, Alhazmi FH, Park DC, Savalia NK, Wig GS. Resting-state network topology differentiates task signals across the adult life span. *J Neurosci*. 2017;37:2734-45.
24. Han L, Savalia NK, Chan MY, Agres PF, Nair AS, Wig GS. Functional parcellation of the cerebral cortex across the human adult lifespan. *Cerebral Cortex*. 2018;28:4403-23.
25. Ewers M, Luan Y, Frontzkowski L, et al. Segregation of functional networks is associated with cognitive resilience in Alzheimer's disease. *Brain*. 2021;144:2176-85.
26. Chan MY, Han L, Carreno CA, et al. Long-term prognosis and educational determinants of brain network decline in older adult individuals. *Nature Aging*. 2021;1(11):1053-1067.
27. Landau SM, Mintun MA, Joshi AD, et al. Amyloid deposition, hypometabolism, and longitudinal cognitive decline. *Ann Neurol*. 2012;72:578-86.
28. Power JD, Mitra A, Laumann TO, Snyder AZ, Schlaggar BL, Petersen SE. Methods to detect, characterize, and remove motion artifact in resting state fMRI. *Neuroimage*. 2014;84:320-41.
29. Franzmeier N, Düzel E, Jessen F, et al. Left frontal hub connectivity delays cognitive impairment in autosomal-dominant and sporadic Alzheimer's disease. *Brain*. 2018;141:1186-200.
30. Avants BB, Tustison NJ, Song G, Cook PA, Klein A, Gee JC. A reproducible evaluation of ANTs similarity metric performance in brain image registration. *Neuroimage*. 2011;54:2033-44.
31. Baker SL, Maass A, Jagust WJ. Considerations and code for partial volume correcting [(18)F]-AV-1451 tau PET data. *Data Brief*. 2017;15:648-57.
32. Schaefer A, Kong R, Gordon EM, et al. Local-global parcellation of the human cerebral cortex from intrinsic functional connectivity MRI. *Cereb Cortex*. 2018;28:3095-114.
33. Yeo B, Krienen FM, Sepulcre J, et al. The organization of the human cerebral cortex estimated by intrinsic functional connectivity. *J Neurophysiol*. 2011;106:1125-65.
34. Marquié M, Normandin MD, Vanderburg CR, et al. Validating novel tau positron emission tomography tracer [F-18]-AV-1451 (T807) on postmortem brain tissue. *Ann Neurol*. 2015;78:787-800.
35. Leuzy A, Chiotis K, Lemoine L, et al. Tau PET imaging in neurodegenerative tauopathies-still a challenge. *Mol Psychiatry*. 2019;24:1112-34.
36. Preische O, Schultz SA, Apel A, et al. Serum neurofilament dynamics predicts neurodegeneration and clinical progression in presymptomatic Alzheimer's disease. *Nat Med*. 2019;25:277-83.
37. Ossenkoppele R, Schonhaut DR, Schöll M, et al. Tau PET patterns mirror clinical and neuroanatomical variability in Alzheimer's disease. *Brain*. 2016;139:1551-67.
38. Vogel JW, Young AL, Oxtoby NP, et al. Four distinct trajectories of tau deposition identified in Alzheimer's disease. *Nat Med*. 2021;27:871-81.
39. Stern Y. Cognitive reserve in ageing and Alzheimer's disease. *Lancet Neurol*. 2012;11:1006-12.
40. Chan MY, Han L, Carreno CA, et al. Long-term prognosis and educational determinants of brain network decline in older adult individuals. *Nat Aging*. 2021;1:1053-67.
41. Kong TS, Gratton C, Low KA, et al. Age-related differences in functional brain network segregation are consistent with a cascade of cerebrovascular, structural, and cognitive effects. *Netw Neurosci*. 2020;4:89-114.
42. Rabin JS, Yang HS, Schultz AP, et al. Vascular risk and beta-amyloid are synergistically associated with cortical tau. *Ann Neurol*. 2019;85:272-9.
43. Dumitrescu L, Mahoney ER, Mukherjee S, et al. Genetic variants and functional pathways associated with resilience to Alzheimer's disease. *Brain*. 2020;143:2561-75.
44. Livingston G, Huntley J, Sommerlad A, et al. Dementia prevention, intervention, and care: 2020 report of the Lancet Commission. *Lancet*. 2020;396:413-46.
45. Chan D, Shafto M, Kievit R, et al. Lifestyle activities in mid-life contribute to cognitive reserve in late-life, independent of education, occupation, and late-life activities. *Neurobiol Aging*. 2018;70:180-3.
46. Lemoine L, Leuzy A, Chiotis K, Rodriguez-Vieitez E, Nordberg A. Tau positron emission tomography imaging in tauopathies: the added hurdle of off-target binding. *Alzheimers Dement (Amst)*. 2018;10:232-6.
47. Lace G, Savva G, Forster G, et al. Hippocampal tau pathology is related to neuroanatomical connections: an ageing population-based study. *Brain*. 2009;132:1324-34.
48. Mu Y, Gage FH. Adult hippocampal neurogenesis and its role in Alzheimer's disease. *Mol Neurodegener*. 2011;6:1-9.
49. Honey CJ, Sporns O, Cammoun L, et al. Predicting human resting-state functional connectivity from structural connectivity. *Proc Natl Acad Sci*. 2009;106:2035-40.
50. Grandjean J, Zerbi V, Balsters JH, Wenderoth N, Rudin M. Structural basis of large-scale functional connectivity in the mouse. *J Neurosci*. 2017;37:8092-101.
51. Abhinav K, Yeh F-C, Pathak S, et al. Advanced diffusion MRI fiber tracking in neurosurgical and neurodegenerative disorders and neuroanatomical studies: a review. *Biochim Biophys Acta*. 2014;1842:2286-97.
52. Harrison TM, La Joie R, Maass A, et al. Longitudinal tau accumulation and atrophy in aging and Alzheimer disease. *Ann Neurol*. 2019;85:229-40.
53. Jack Jr., CR, Wiste HJ, Schwarz CG, et al. Longitudinal tau PET in ageing and Alzheimer's disease. *Brain*. 2018;141:1517-28.
54. Brown BM, Rainey-Smith SR, Dore V, et al. Self-reported physical activity is associated with tau burden measured by positron emission tomography. *J Alzheimers Dis*. 2018;63:1299-305.
55. Buckley RF, O'Donnell A, McGrath ER, et al. Menopause status moderates sex differences in tau burden: a Framingham PET study. *Ann Neurol*. 2022;92:11-22.
56. Franzmeier N, Ossenkoppele R, Brendel M, et al. The BIN1 rs744373 Alzheimer's disease risk SNP is associated with faster Abeta-associated tau accumulation and cognitive decline. *Alzheimers Dement*. 2021;18(1):103-115.
57. Franzmeier N, Rubinski A, Neitzel J, Ewers M, Alzheimer's Disease Neuroimaging I. The BIN1 rs744373 SNP is associated with increased tau-PET levels and impaired memory. *Nat Commun*. 2019;10:1766.

58. Maass A, Landau S, Baker SL, et al. Comparison of multiple tau-PET measures as biomarkers in aging and Alzheimer's disease. *Neuroimage*. 2017;157:448-63.

SUPPORTING INFORMATION

Additional supporting information can be found online in the Supporting Information section at the end of this article.

How to cite this article: Steward A, Biel D, Brendel M, et al. Functional network segregation is associated with attenuated tau spreading in Alzheimer's disease. *Alzheimer's Dement*. 2023;19:2034–2046. https://doi.org/10.1002/alz.12867